Measurement 242 (2025) 116030

Contents lists available at ScienceDirect

Measurement

journal homepage: www.elsevier.com/locate/measurement

In-field assessment of bridge pier scour by means of Fiber Bragg Gratings: System and algorithms

Gianluca Crotti [a], Stefano Manzoni [b,*]

[a] Politecnico di Milano, Dept. of Civil and Environmental Engineering, Piazza Leonardo da Vinci 32, 20133, Milano, Italy
[b] Politecnico di Milano, Dept. of Mechanical Engineering, Via La Masa 1, 20156, Milano, Italy

ARTICLE INFO

Keywords:
Scour measurement
Scour monitoring
Bridge monitoring
Scour device
Hydraulic device
Bragg grating sensor

ABSTRACT

BLESS (Bed LEvel Seeking System) is a sedimeter that measures riverbed level around bridge pier in water. It is based on Fiber Bragg Gratings and the working principle is based on the measurement of the different heat dissipation behaviour in the saturated soil compared to the flowing water. It is an innovative part of a complex monitoring system installed on a road bridge over the Po river (Italy). After two years of data storage, a comparison of two different methods to detect the riverbed level can be performed. One of them showed results in satisfactory agreement with those provided by a traditional reference device, i.e., an echo sounder. Furthermore, coupling the two different proposed bed level estimation methods allows deriving significant information about the health status of the sedimeter. The device is reliable enough to operate and survive in very harsh environments and it is ready for further engineering applications.

1. Introduction

The riverbed level is the most important quantity to assess pier and, therefore, bridge stability during flood events [1], when it is not so rare to record bridge failures [2–4]. The bed of the river around piers is interested, especially during floods, by a process called local scour [5]: it removes sediments all around the submerged structure creating a scour hole that decreases the ground level locally and increases the forcing actions applied to the pier. This process is the main reason for bridge collapse [6] and, for such a reason, real-time monitoring of pier scour is very important. Furthermore, the possibility to monitor such a quantity is also able to provide significant information for prediction of scour level in near future by means of artificial intelligence approaches [7]. It is also noticed that the problem of scouring is related also to other types of structure (e.g., offshore structures [8,9]). Its importance in terms of the safety of people and infrastructures is therefore evident.

At present, there are different ways to estimate the riverbed level at piers: (i) development of theoretical models based on laboratory experiments, (ii) use of numerical models and machine learning approaches (e.g., [10–12]), and finally (iii) the use of specific devices to directly measure the depth of the bed [13], at least during floods.

In the first case, one has to consider that the local scour process is generated by a three-dimensional turbulent flow field that involves several factors like different sediment layers and sizes, pier geometry, river morphology in continuous time development, velocity field around pier that changes with water level, etc. All these variables are now not included in prediction models (or they are included but with strong simplifications) so that an accurate estimation is not guaranteed [14]. Moreover, if the specific case is very complex in term of pier geometry and river morphology compared to the laboratory set-up, a field check of the output of the model is suggested. In the second case, the computational burden can be very high, preventing real-time monitoring, and the accuracy of the numerical model still represents an important issue for the success of the scour estimation. These points imply that an accurate assessment of the river bed level through models is still difficult or even not completely feasible in practical applications. For these reasons, a monitoring system is necessary to check the bridge safety [15], especially during floods.

The third approach relies on the measurement of the level of the riverbed. In the last ten years, the literature is rich of examples where devices have been tested in laboratory or in field [16–18]: from temperature measurements [19,20] to reflectometry [21,22] and smart magnetic rocks [23,24], from vibration-based [25–27] to image-based approaches [28]. At present, there are many devices that can be used to measure the riverbed level but none of them can be considered as a standard because they present advantages and disadvantages depending

* Corresponding author.
E-mail addresses: gianluca.crotti@polimi.it (G. Crotti), stefano.manzoni@polimi.it (S. Manzoni).

https://doi.org/10.1016/j.measurement.2024.116030
Received 5 February 2024; Received in revised form 3 July 2024; Accepted 17 October 2024
Available online 19 October 2024

on the specific case [29]. Probably, currently, the most used device is the echo-sounder [30]. As reported by [29] and [2], the echo-sounder is not expensive and easy to install but its performance is strictly related to the distance between itself and the riverbed. Moreover, its working principle (sonic pulse reflected by the riverbed) has limitations depending on the presence of debris, high sediment transport and air entrapment. These conditions can either alter the signal, implying the need of complex data processing, or block completely the ultrasonic pulse in the worst situations [31]. To overcome such problems, at least two devices with different working principle have to be employed, performing a cross check to guarantee a continuous monitoring.

One promising approach to directly measure riverbed level is the use of fiber optic sensors (e.g., [32]), that allows solving different problems related to the harsh environment. Being fiber optics extremely thin, they can be easily protected and placed close to piers. Furthermore, working with light signals, they do not suffer of usual problems affecting electrical devices in wet environments. Fiber optic sensors can be used to the aim of bridge scour estimation employing them as either temperature sensors (e.g., [33,34]) or strain sensors (e.g., [35–38]). In 2011, a fiber optic sedimeter, named BLESS (Bed LEvel Seeking System) [39] was proposed. This device was installed on a road bridge, in Borgoforte, over Po stream, the longest Italian river, to measure the riverbed level. After two years of data acquisition, an analysis can be now carried out with two different aims: (i) find automatic algorithms to evaluate the riverbed level in any condition and (ii) find approaches for monitoring the health condition of the BLESS. These are key points towards the use of BLESS on further bridges. To this purpose, data acquired at Borgoforte system will be used. These data were collected between 2012 and 2013 but have been made available only recently. This paper also constitutes the occasion to evidence which are the main difficulties in passing from lab [39] to a real application where a number of additional issues must be taken into account: from the protection of the measurement device from the harsh environment (see Section 3) to the development of new algorithms able to assess the bed level in complex working conditions (see Sections 4 and 5).

The paper is structured as follows: Section 2 recalls the basic working principle of Fiber Bragg Gratings (FBGs) which are at the base of BLESS functioning, and Section 3 presents the Borgoforte Bridge, the monitoring system and BLESS, focusing on its data output. Then, Section 4 describes the pre-processing of data coming from BLESS, while Section 5 proposes methods to find the riverbed level and discusses the results related to two years of data collection, also suggesting an approach for monitoring the health condition of BLESS.

2. Working principle of FBGs

FBGs can be used for measuring both temperature and strain. The measurement is carried out by detecting the shift $\Delta\lambda$ of the Bragg wavelength λ_b due to presence of strain ε and variations of temperature T:

$$\frac{\Delta\lambda}{\lambda_b} = k_g(\varepsilon_m + \varepsilon_T) + \alpha(T - T_{ref}) \quad (1)$$

where k_g is the gage factor, α expresses the change of the refractive index per unit of temperature, ε_m is the strain generated by mechanical actions and ε_T is that due to thermal changes. Finally, T_{ref} is a reference temperature at which the Bragg wavelength is at λ_b when ε_m is null.

Under a general point of view, the main advantages offered by FBGs compared to traditional transducers are related to (i) the small size which implies no load effect and ease of insertion in systems and structures, and (ii) capability to work in harsh environmental conditions such as, e.g., presence of water, magnetic fields, chemical substances (see, e.g., [40–45]).

In the present application, those advantages translate into the possibility of having sensors properly working when immersed in water and of easily attaching FBGs to the piers and protecting them from debris. In this case, FBGs are expected to perform temperature measurements, which implies that it is needed to prevent possible strain influence on the FBG output signals. This point is treated in Section 3.

3. Borgoforte bridge, monitoring system and BLESS

The bridge under consideration is located in Borgoforte, Italy, over Po, the longest Italian river (Fig. 1). The hydraulic history and a detailed description of this bridge can be found in [46] and [47], respectively. The monitoring system was installed on the pier 30 (Fig. 1) in 2011 (more details about the reason why the system was installed on the pier close to the bank can be found in [46]). The underlying approach of this monitoring system is quite different compared to other classic structural health monitoring methods because it is based on the measurement of active forces on the bridge and not on the response of the structure. The reader can find details about this choice in [47].

The riverbed detection, which is the focus of this paper, is made from a standard ultrasonic device (echo sounder) and BLESS; the latter is the focus of this paper. The echo sounder was initially added to the system to check the reliability of BLESS in field applications since this was the first time it was installed on a real bridge.

BLESS is a patented sedimeter [48], which means that it must be in contact with the measured environments: wet sediment and flowing water. It is based on many FBGs, whose number and spacing are customizable, placed along the same fiber optic that is laid along the monitored pier. A complete description of the working principle is available in [39] and, here, it will be summarized for the sake of comprehension of this new work.

The Borgoforte system layout is presented in Fig. 2. In picture (a) a panoramic view of the pier 30 is provided. Downstream the pier there is the support of BLESS (i.e., of the optical fiber containing the FBGs). The whole system is composed by a control box (at road level) and a stainless steel tube split in two parts: the upper one, tube 1, protects the connections between the control box and BLESS, while part 2 (tube 2), which starts at the lowest horizontal beam, is the actual support of BLESS. The control box contains the interrogation system for the FBGs and a power supplier used to heat the FBGs, as explained further in the manuscript. The echo sounder is placed at the end of tube 2.

Looking at tube 2 from downstream, the layout of BLESS is shown in Fig. 3(a). The BLESS device (in black) is covered by a rigid protection (to avoid debris impacts) except for the parts where the FBGs are located. Fig. 3(b) offers a simplified sketch of this configuration.

The black color of BLESS is due to heat shrinkable material covering the real system. Inside the heat shrinkable slice, the optical fiber and an electrical wire are present. The electrical circuit starts at one pin of a power supplier, placed in the control box of Fig. 2(a), goes down to the end of the optical fiber and, then, climbs back to the other pin of the power supplier. It is used to heat the FBGs by means of Joule's effect when the mentioned power supplier is switched on (see [39] for more details). When the power supplier is turned on, all the FBGs sense a temperature increment, while they sense the temperature of the environment in which they are (either water or soil) when the supplier is turned off.

When FBGs are heated, the increment of the FBG response and its speed depend on the environment in which the sensor is immerged: flowing water or saturated soil (see the next section for a quantitative analysis). Considering the sketch in Fig. 3(b), it is possible to explain, qualitatively, how BLESS can define the level of the riverbed. Each black square is an FBG heated with a heat power step: being FBGs temperature sensors, their response behave, approximately, like that of a first order system [39], resulting in a step response dependent on a negative exponential function [49] (see further in the paper). The behavior of this step response is strongly influenced by the boundary conditions of the considered FBG. Indeed, the overall increment of sensed temperature increases when the FBG is in soil compared to the case it is in water,

Fig. 1. Borgoforte road bridge during a flood in 2018. The river Po flows from left to right.

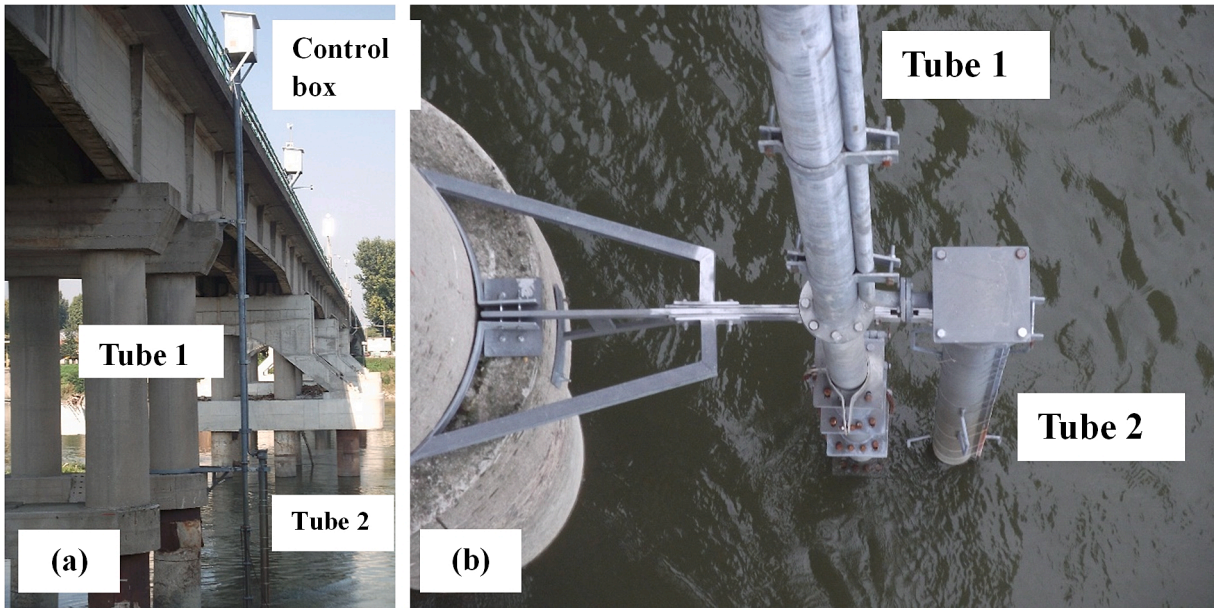

Fig. 2. (a) The pier 30 and the BLESS constructions: control box, shelter (tube 1) and BLESS support (tube 2). (b) A zoom of tube 2.

while its speed decreases. This is mainly due to the different mechanisms of heat dissipation in water (convection) and soil (conduction). Therefore, referring to Fig. 3(b), the first five sensors (from the top) nominally provide the same step response (because all of them are in water). The remaining four FBGs show again similar step response because they are all in soil. However, the response of the first five FBGs will be different in terms of amplitude and speed compared to that of the remaining FBGs. Analyzing these differences, it is possible to assess the condition of each FBG (i.e., either in water or in soil) and, thus, to derive the river bed level. Therefore, BLESS does not give the exact level of the bed but an interval in which it is located. This range is strictly correlated to the customizable spacing among FBGs, from few centimeters to meters depending on the specific application. Furthermore, it is noticed that the resolution of the bed level estimation can be even improved [33] using fiber optic-based distributed temperature sensing. The core of BLESS system is the algorithm to analyze data and to estimate in which environment every FBG is immerged (see further in the manuscript). Furthermore, another related key point is to guarantee at least the minimum power supply that a generic FBG needs in order to have a clear separation of thermal responses in flowing water and saturated soil.

According to the authority in charge of Borgoforte bridge, the maximum scour hole registered around a pier is approximately 10 m, and the normal fluctuation of the riverbed is about 2 m. Therefore, the portion of BLESS where 34 FBGs are placed is 26 m long (not only to cover the potential scour but also to have additional sensors in the water and in the soil). The spacing between adjacent FBGs for the first fifteen sensors (from the top) is 0.5 m while for the rest is 1 m. The total length of BLESS is 49 m considering the connection with the control box (Fig. 2).

The thermal power P produced by the Joule's effect in

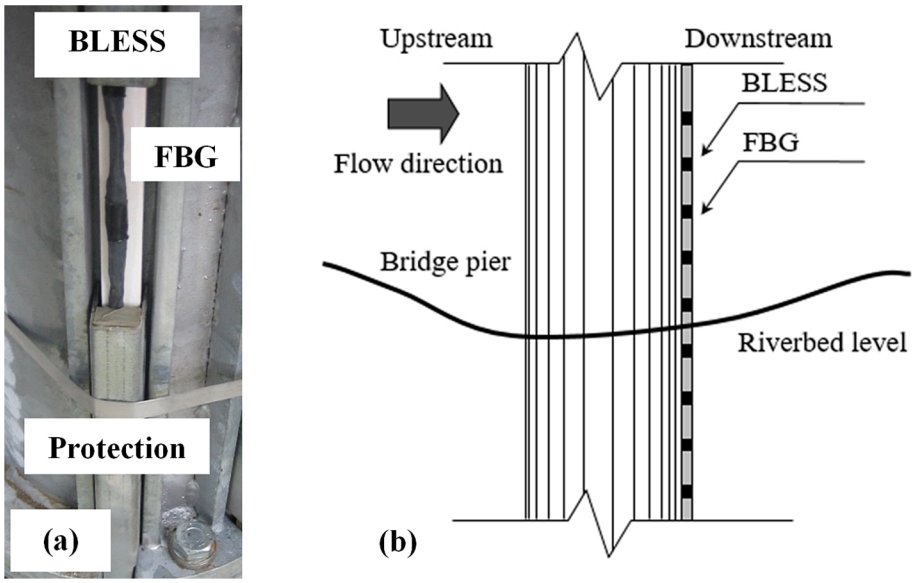

Fig. 3. BLESS system layout. (a) A picture of BLESS showing that only FBG is exposed to the environment. (b) A simplified sketch where each black square is an FBG.

correspondence of each FBG can be easily estimated as $P = R{\cdot}I^2$, where R is the electrical resistance in correspondence of the FBG and I is the constant current flowing in the electrical circuit. To find a good balance between the thermal power provided to each FBG and the power produced by the power supplier, the electrical circuit was built using two different types of electrical cable. A low-resistance one ($\rho_1 = 0.06$ Ω/m, where ρ indicates electric resistance per unit of length) used for areas where there is no FBG, and a high-resistance cable ($\rho_2 = 26$ Ω/m) in correspondence to the location of each FBG (total length of 5 cm around each sensor). Therefore, the electrical circuit results in the series of short-length wire pieces with different electrical resistance value.

Since the power supplier produces a voltage of 48 V and the measured total resistance of the whole electrical wire is 110 Ω (with a resulting current I of 0.44 A), the resulting thermal power produced at each piece of high-resistance cable is approximately equal to 0.25 W (i.e., 0.25 W/FBG). Since two pieces of high-resistance cable are present in correspondence of each FBG (because the electrical wire travels along BLESS from the top to bottom and again to the top, see previously), the thermal power produced at each FBG is doubled: about 0.5 W (i.e., 0.5 W/FBG). According to Manzoni et al. 2011 [39], at least 1.2 W/FBG are needed for a clear distinction between soil and flowing water. Therefore, three wires in parallel have been used at Borgoforte system, having a final power P value of 1.5 W/FBG.

The BLESS is activated four times a day and the power unit is turned on for 200 s every time. The sampling frequency used to collect the responses of all the FBGs is 1 Hz. In this way, BLESS collects FBG responses for a time long enough to discern between water and soil for each FBG (see Section 4). At the same time, the data to transmit with wi-fi protocols from bridge to remote station do not have an excessive size.

The next subsection gives details about the mathematical formulation to describe the signal provided by an FGB when the power supplier is switched on.

Before proceeding, it is however essential to face another point: FBGs are sensitive not only to temperature but also to strain (see Section 2). Therefore, for temperature measurements, it is essential to prevent possible strain influence on the FBG output signals. There are different approaches to guarantee it, e.g., [50]. In this case, uncoupling between thermal and strain effects was achieved by using a commercial layout where the fiber is placed inside a tailored structure constituted by a sequence of aluminum tubes and flexible rubber tubes. The FBGs are in correspondence of the aluminum tubes for improving safety from impacts. The fiber was fixed in correspondence of each aluminum tube and it was left loose between subsequent junction points. All this system was then surrounded by heat shrinkable material for protection from water. This solution was also tested in laboratory before installation at the bridge with satisfactory results in terms of non-sensitivity to strain.

3.1. Step response and main parameters

In Manzoni et al. [39], BLESS response was described as the response to a step of dissipated power (obtained by means the Joule's effect, as mentioned). Such a response can be approximated as the response of a first order system (see Fig. 4).

More in detail, at the beginning (from $t = 0$ s to t_0, where t indicates time) the FBG measures the temperature of the environment (T_{ENV}) because no heating is imposed. At t_0, a step of the dissipated power (obtained by switching on the power supplier at 48 V) is imposed, which approximately corresponds to a thermal step ΔT (black solid line in Fig. 4). The FBG response is collected from t_0 for a time long enough to describe the first order system response to a step function (dashed line in Fig. 4). Data acquisition is stopped at t_{end}, and the power supplier is then switched off. As mentioned, the FBG response shows a behavior close to that of a first order system and, thus, waiting enough time, the system,

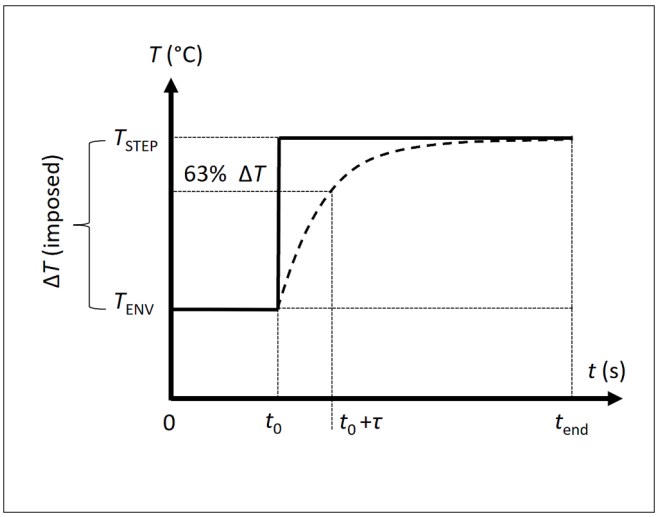

Fig. 4. Step response of a first order system.

slowly or quickly, reaches the steady state at $T_{STEP} = T_{ENV} + \Delta T$. The equation of this response (dashed line in Fig. 4) is:

$$T(t) = T_{ENV} + \Delta T\left(1 - e^{-(t-t_0)/\tau}\right), \quad t \geq t_0 \tag{2}$$

where T is the temperature provided in output by the FBG, ΔT is the imposed temperature step $T_{STEP} - T_{ENV}$ and τ is the time constant which represents the time needed to the response to reach approximately the 63% of ΔT [49] (see Fig. 4).

Fig. 5(a) shows typical experimental FBG responses to the heating for both environments in which the sensor can be immerged: flowing water (FBG 4 in Fig. 5) and saturated soil (FBG 5), with the best fitting curves (using Eq. (2)) in Fig. 5(b). Thus, both the time histories are related to a real acquisition from Borgoforte monitoring system. Compared to Fig. 4, in Fig. 5 the time starts when the heating is turned on (t_0 in Fig. 4 is 0 s in Fig. 5). All the curves of Fig. 5 are shifted vertically so that $T_{ENV} = 0$ for an easier comparison. The same electric circuit heats all the FBGs, so that the imposed thermal power step is nominally the same for every sensor. Conversely, the corresponding thermal jump ΔT is different due to the environment in which the FBG is located (in Fig. 5 the ΔT of sensor 5 is approximately the double compared to that of FBG 4).

The field results, plotted in Fig. 5, can also be used to understand the impact of the environment on the FBG responses. In flowing water, the heat generated by the electrical circuit is dissipated by convection; on the contrary, the conduction is the main process for heat dissipation in the riverbed. Convection is more efficient compared to the conduction so that ΔT and τ are lower in water (lower τ value means quicker step response). These two parameters are thus at the base of most scour detection methods based on temperature measurements in presence of external power sources [19,20,33,39]. When thermal power is produced, as in this case, the method is usually referred to as active thermometry [20]. In contrast, when no external power source is employed, the method is referred to as passive thermometry [20]. However, the latter approach suffers from the disturbing effects related to seasonal environmental variations [20] resulting in more problematic practical implementation. Under a theoretical point of view, using active thermometry, the ΔT and τ values would be enough for assessing scour level. However, according to [39], this occurs only when large thermal power values are used, which is unfeasible in practical applications. Indeed, in the present case, the involved thermal power (i.e., 1.5 W/FBG, see previously) is much less than that employed in, e.g., [20]. For this reason, the use of ΔT and τ indexes will not be sufficient in this real application for achieving large result reliability (even if the dissipated thermal power is larger than the theoretical threshold of 1.2 W/FBG given in [39]), as evidenced further in the paper.

It is also important to notice that the responses in Fig. 5a (and all the temperature data obtained by FBGs and used in this paper) were derived using the nominal sensitivity provided by the sensor manufacturer. Even if a calibration would improve the metrological behaviour of each FBG, this task is assumed as non-feasible in a real application for constraints in time and resources.

4. Data pre-processing

This section introduces how to pre-process data to the aim of detecting the riverbed level at the pier where BLESS is installed. To this purpose, the signals in Fig. 5 are used as examples. For more details about the content of this section, the interested reader can also refer to [31].

If the goal is to evaluate the different responses in terms of the parameters involved, ΔT and τ, to understand where the FBGs are (flowing water or saturated soil), heating must be provided for a sufficient time to guarantee the complete representation of the step responses. In other words, steady state must be reached before data acquisition and heating are stopped. In Borgoforte, as mentioned before, the heating time is 200 s (Fig. 5), and the thermal power step is set to 1.5 W/FBG. In Table 1, the values of ΔT and τ for sensors 4 and 5 plotted in Fig. 5 are presented.

The measured ΔT is calculated for t equal to 200 s. The curves in Fig. 5(a) and the corresponding values in Table 1, related to the two sensor responses, are different: ΔT of FBG 5 is about the double of that related to FBG 4 and τ of FBG 5 is approximately 50% larger than τ of FBG 4. According to BLESS working principle (see [39]), this allows concluding that FBG 4 is in flowing water while FBG 5 is buried in the river bed. Similar outcomes are obtained from the other sensors of BLESS installed in Borgoforte and, therefore, it is in theory possible to use the values of ΔT and τ to find the bed level. However, an additional point deserves attention. The 34 FBGs in BLESS are not calibrated (the nominal sensitivity given by the manufacturer and equal for all the FBGs is used) and, thus, one sensor could show a different output compared to another one even though they are in the same environment with the same temperature. This bias can be in the order of few degrees Celsius. More generally, each FBG shows a slightly different behavior compared to the others. This implies that, in a real application, it is not possible to find the same ΔT value for all the FBGs in soil and another given value for all the FBGs in water, so that the FBGs in a given environment

Table 1
Main parameters of sensors 4 and 5 plotted in Fig. 5.

FBG	Measured values		Fit of the experimental response with Eq. (2)	
	ΔT (°C)	τ (s)	ΔT (°C)	τ (s)
4 in water	3.08	39	2.90	40
5 in soil	5.99	61	6.14	65

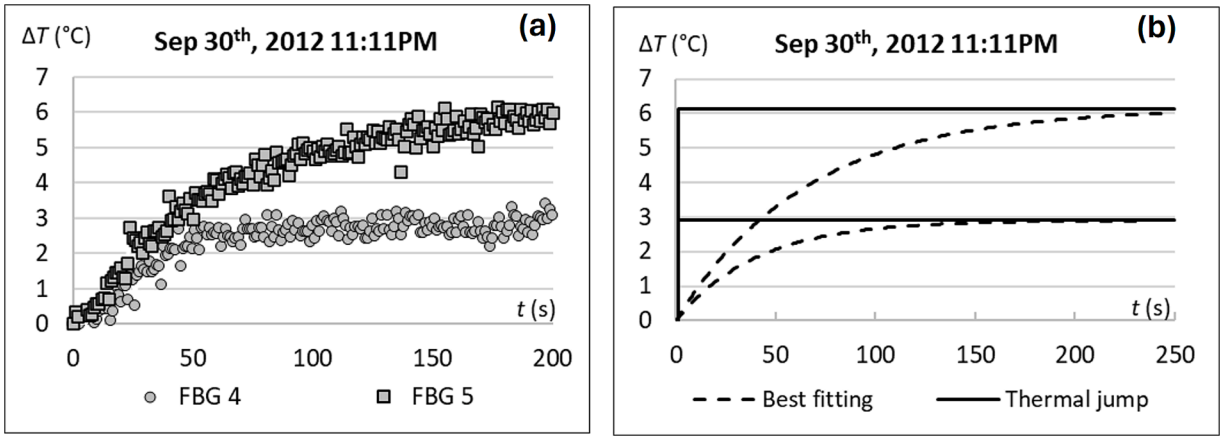

Fig. 5. (a) Field acquisition in flowing water (FBG 4) and saturated soil (FBG 5); (b) thermal step and best fitting (see Fig. 4 and Eq. (2)).

describe an interval of ΔT values. The same applies to the τ values. This poses some issues for a proper comprehension of which sensors are in soil and which are in water, in turn making it difficult to properly estimate the riverbed level. To overcome this issue, the next subsections will present some interesting parameters that can be extracted, which will be then used in Section 5 for estimating the riverbed level. These subsections will also discuss some examples, remarking that the slightly different behaviors of all the FBGs generate problems for a straightforward estimation of the bed level directly from step responses.

More in detail, Section 4.1 will discuss whether the estimation of the ΔT and τ values provided by all the FBGs can be used for a reliable estimation of the riverbed level. In this subsection, each FBG response is considered alone. Conversely, in Section 4.2, the ΔT and τ values obtained from adjacent FBGs (e.g., for FBG number 1, the adjacent FBG is number 2, then 2 and 3, and so on) are compared to extract further parameters, named $\Delta\Delta T$ and $\Delta\tau$, useful for the bed level detection.

4.1. Single FBG parameters

Fig. 6 shows the curves of the first nine sensors with the corresponding ΔT and τ values for a generic acquisition, as an example for the following discussion. According to echo sounder output, the first four sensors are in flowing water (solid black curves) and the others are in the soil (red dashed curves).

According to Fig. 6 and as discussed before, the temperature increment ΔT in the water is smaller compared to the increment in the soil. Furthermore, the time constant in water results smaller than that in soil. Therefore, it is possible to set two thresholds, one for each parameter, in order to assign all nine sensors to one of the two environments. From here on, ΔT_{T} will indicate the threshold for the ΔT parameter, while τ_{T} will indicate the threshold for τ.

Fig. 7 shows the ΔT and τ values as function of the sensor number for the FBG responses of Fig. 6. Considering the ΔT plot (plot (a)), it is evident that the first four sensors are in flowing water because they are characterized by smaller values compared to the rest of the sensors, which are thus in soil. This is in agreement with the echo sounder output.

Moreover, it is straightforward to conclude that the riverbed level (grey layer) is between sensors 4 and 5 because a ΔT jump occurs. The same behavior is showed in Fig. 7 (b) for the time constant τ: the τ jump is, again, between sensors 4 and 5 even though the dispersion of the τ values in soil is significant.

Therefore, a threshold smaller than the minimum value related to the FBGs in the soil (from 5 to 9) and, at the same time, greater that the maximum value for the sensors in water (1 to 4) can be set for both ΔT and τ. In this way, it is possible to move every sensor into a specific environment ($2.90 < \Delta T_{\mathrm{T}} < 5.57$ °C and $40 < \tau_{\mathrm{T}} < 50$ s for this specific case; see the grey layers in Fig. 7) for the subsequent acquisitions. However, a single set of time histories is not enough to set the thresholds and a calibration dataset is needed. To this purpose, all the field data of 2012 (about 267 acquisitions) were used to build the calibration dataset.

Fig. 8 shows, for the first nine FBGs, the range of ΔT and τ values for 2012 (represented by the line between two black squares). Considering the ΔT plot (plot (a)), the sensors showing a low variation (solid line) are those that were in the same environment for all the acquisitions (FBGs 1 to 3 in the water and 6 to 9 in the soil).

Even though the environment conditions can change with time (e.g., the velocity of water), these variations cannot strongly alter the FBG response and, thus, the interval of the recorded values is small. Conversely, the sensors having a large range variation (dashed line, i.e., sensors 4 and 5) are those that were immerged in both environments (water and soil) during the time of the acquisitions. In this case, the ΔT parameter has a larger variability. The results of Fig. 8(a) allows defining a new and more reliable grey area to distinguish FBGs in soil and in water (i.e., $3.6 < \Delta T_{\mathrm{T}} < 5.3$ °C) which can be used when analyzing data different from those of 2012.

Considering τ (see Fig. 8(b)), there is always an overlap between the FBG ranges, probably because the time constant is more sensitive to disturbing variables (e.g., environmental temperature). Therefore, it is possible to conclude that, in this specific case, the ΔT value is a quantity practically usable to detect the riverbed, while the time constant must be discarded.

4.2. Adjacent FBG parameters

If two consecutive FBGs are considered, two cases are possible: (i) the sensors are in the same environment (i.e., either water or soil) or (ii) the sensors are in different environments. In the first case, the difference between the two values of ΔT, that is $\Delta\Delta T$ ($\Delta\Delta T_{i+1,i} = \Delta T_{i+1} - \Delta T_i$, being i a counter on the FBGs), is close to zero (see previously) and the same applies to $\Delta\tau$ ($\Delta\tau_{i+1,i} = \tau_{i+1} - \tau_i$). In the second case, the sensors are in different environments and the values of $\Delta\Delta T$ and $\Delta\tau$ are expected to be largely positive. Table 2 shows the values of the parameters $\Delta\Delta T$ and $\Delta\tau$ evaluated for the curves of Fig. 6, while Fig. 9 gives a graphical representation of the same values.

Using $\Delta\Delta T$, it is possible to find the level of the riverbed, see the grey arrow in Fig. 9(a), between sensors 4 and 5, corresponding to the $\Delta\Delta T$ maximum value. As for $\Delta\tau$, it is still possible to detect the river bed level (see the grey arrow in Fig. 9(b)) even if there are possible anomalous behaviors like that between FBGs 5 and 6 in Fig. 9(b), where the large negative value is probably due to a change of soil properties. The advantage of the two parameters described in this subsection is the absence of a threshold value. This implies that there is no need of a period of time where data acquisition is devoted to threshold estimation. Indeed, for each new acquisition, the riverbed is detected looking for the maximum value of either $\Delta\Delta T$ or $\Delta\tau$.

FBG	ΔT (°C)	τ (s)
1	1.50	32
2	1.41	34
3	2.79	40
4	2.90	40
5	6.14	65
6	7.32	50
7	6.22	62
8	5.57	63
9	7.19	55

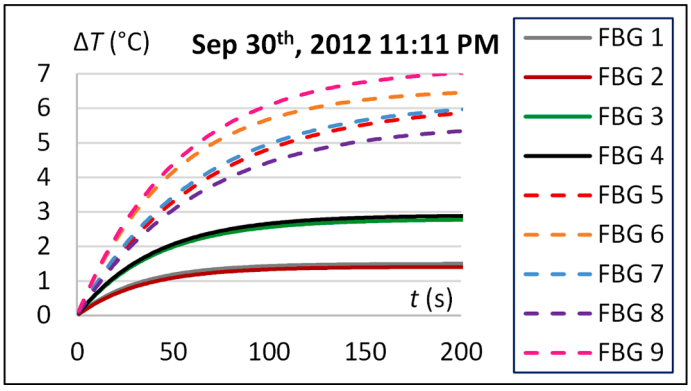

Fig. 6. Field acquisition. The parameter values obtained from the fit with Eq. (2) and the corresponding curves: dashed lines for FBGs in soil (FBGs 5 to 9) and solid lines for FBGs in water (FBGs 1 to 4).

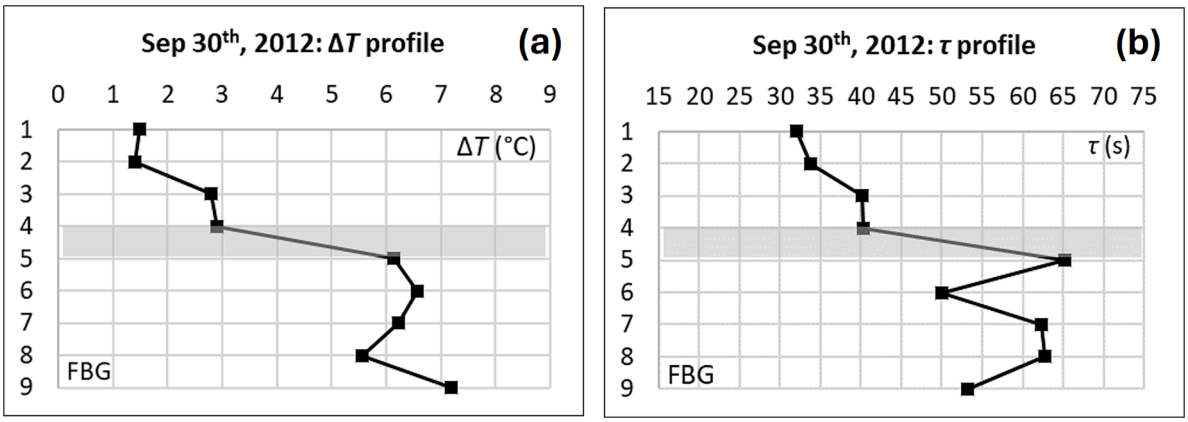

Fig. 7. ΔT (a) and τ (b) values for the step responses in Fig. 6. The grey zone indicates the location of the riverbed.

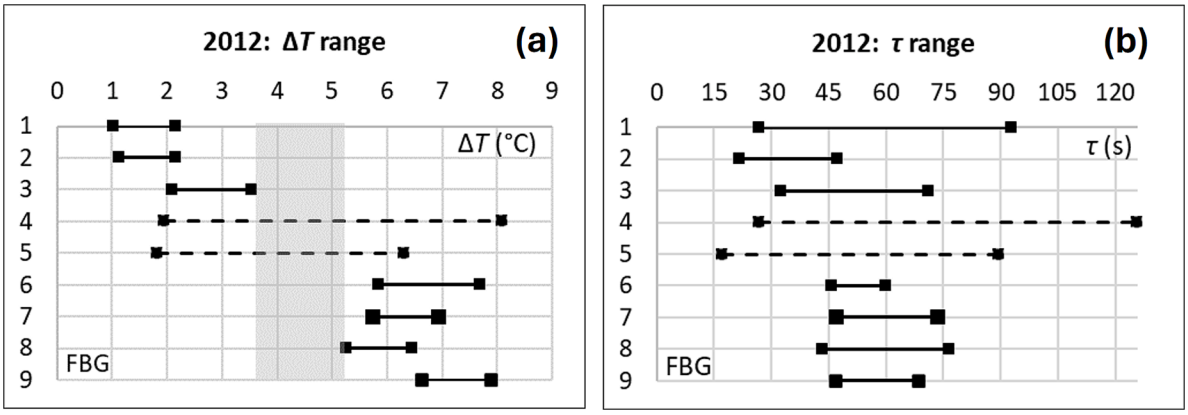

Fig. 8. ΔT (a) and τ (b) range (min and max values recorded for the entire 2012).

Table 2
$\Delta\Delta T$ and $\Delta\tau$ values calculated for the nine FBG step responses of Fig. 6.

	Adjacent Sensors							
	2,1	**3,2**	**4,3**	**5,4**	**6,5**	**7,6**	**8,7**	**9,8**
$\Delta\Delta T$ (°C)	−0.09	1.38	0.11	**3.24**	1.18	−1.10	−0.65	1.62
$\Delta\tau$ (s)	2	6	0	**25**	−15	12	1	−10

The quantities defined in this and previous subsection (i.e., ΔT, $\Delta\Delta T$ and $\Delta\tau$) will be used in the next section to design and test two refined approaches for a reliable detection of the riverbed level. It will be shown that one of them shows superior performances. Nonetheless, the less effective approach will be useful to assess the health condition of BLESS.

5. Two methods for detecting the riverbed level

In the previous section, three possible parameters have been identified for the estimation of the riverbed level: ΔT, $\Delta\Delta T$ and $\Delta\tau$.

The goal of the analysis of this section is to find highly reliable automatic methods for riverbed detection. One method uses all the three available parameters and it is based on a physical approach (see Section 5.1). Basically, the riverbed level is estimated with this method by means of different physical parameters. Among them, the main ones are

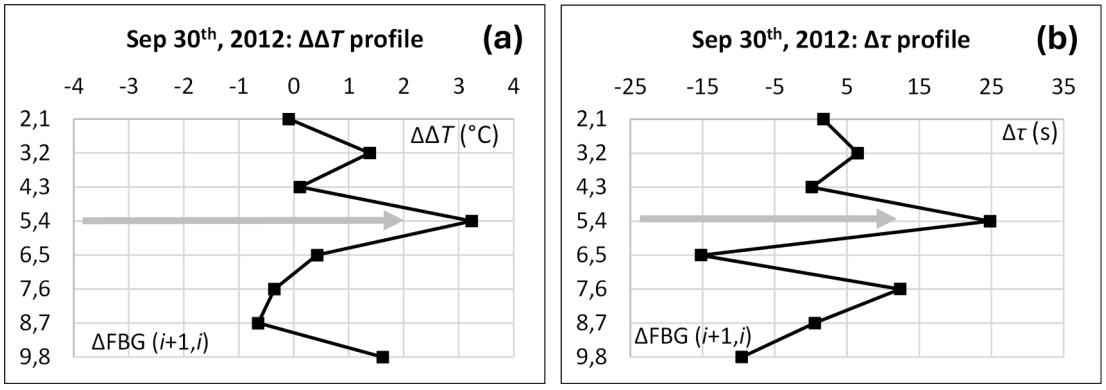

Fig. 9. $\Delta\Delta T$ (a) and $\Delta\tau$ (b) values of Table 2. The symbol ΔFBG used as label of the vertical axes indicates which pair of FBGs is considered. As an example, 2,1 indicates that $\Delta\Delta T$ is measured between FBGs 2 and 1 (i.e., $\Delta\Delta T_{2,1}$).

linked to thermal gradients with respect to both time (ΔT) and space ($\Delta\Delta T$). This method is, thus, based on Gradient Knowledge and is named GK method. In addition, a different method, named DC method and employing Data Clustering, is discussed in Section 5.2. This second method does not rely on any physical underlying consideration and uses only one of the three above parameters.

5.1. GK method

As mentioned, this method uses all the three available parameters: ΔT, $\Delta\Delta T$ and $\Delta\tau$. Since the parameter τ was shown to be not reliable for riverbed detection in Section 4.1 due to its large scatter, here the value of $\Delta\tau$ is considered less reliable than those of ΔT and $\Delta\Delta T$. Hence, these two latter parameters are mainly employed here, and the value of $\Delta\tau$ is used only if needed.

The riverbed level is defined when the ΔT result corresponds to the $\Delta\Delta T$ one (i.e., the bed level detected with ΔT is equal to the bed level detected with $\Delta\Delta T$). The spatial accuracy of this estimation of the riverbed level is obviously related to the spacing between the two sensors involved. Conversely, in case the results provided by the parameters ΔT and $\Delta\Delta T$ are different, $\Delta\tau$ is considered: if $\Delta\tau$ indicates the riverbed level as equal to one of those indicated by either ΔT or $\Delta\Delta T$, the bed level is estimated as that indicated by $\Delta\tau$. In case all three results are different, the use of $\Delta\tau$ is avoided and the bed level is estimated accounting for the results indicated by ΔT and $\Delta\Delta T$, thus with a worsened level of spatial accuracy. As an example, if ΔT indicates bed level between FBGs 2 and 3, $\Delta\Delta T$ between FBGs 3 and 4, and $\Delta\tau$ between FBGs 4 and 5, finally bed level is assumed between FBGs 2 and 4.

Being this method based on the descriptions and assumptions discussed in Sections 4.1 and 4.2., it is possible to conclude that its working principle is laid down on considerations related to the physical phenomena at the base of BLESS functioning. Furthermore, it is noticed that, since the estimation of the riverbed level through the parameter ΔT requires a calibration (see Section 4.1), the use of GK method needs to carry out a training on a given amount of time.

5.2. DC method

DC method is an application of K-Means Clustering Algorithm [51]. A generic clustering algorithm is an independent method to analyze data: its aim is to create groups of data (clusters) for obtaining similar groups. In this specific case, a dataset containing the ΔT values of the FBGs has to be classified, distinguishing between FBGs in flowing water and in saturated soil, using the thermal distance defined below as similarity function.

To understand the method, the reader can refer to Fig. 10 that uses the ΔT values of Fig. 6 (nine sensors) as an example. In STEP 1, the number of FBGs, their ΔT values and a preliminary separation of sensors

STEP 1 - Separation of FBGs into two groups - first attempt

FBG	1	2	3	4	5	6	7	8	9
ΔT [°C]	1.50	1.41	2.79	2.90	6.14	6.07	6.22	5.57	7.19
Field	water		soil						

STEP 2 – Definition of centroids, evaluating thermal distances, new field assignation

ΔT_{mean} [°C]	1.45		5.27						
TD_{water} [°C]	0.05	0.04	1.34	1.45	4.69	4.62	6.77	4.12	5.74
TD_{soil} [°C]	3.77	3.86	2.48	2.37	0.87	0.80	0.95	0.30	1.92
Field	water				Soil				

STEP 3 – Equal to STEP 2 (iteration loop)

ΔT_{mean} [°C]	2.15				6.24				
TD_{water} [°C]	0.65	0.74	0.64	0.75	3.99	3.92	4.07	3.42	5.04
TD_{soil} [°C]	4.74	4.83	3.45	3.34	0.10	0.17	0.02	0.67	0.95
Field	water				soil				

STEP 4 –Iteration loop

ΔT_{mean} [°C]	2.15	6.24

Fig. 10. DC method logic.

(e.g., the first two FBGs are in water and the rest into the soil) are defined. Then, STEP 2 analyses if a sensor is in the right group, otherwise it must be placed in the other one. In detail, the mean value of ΔT for the two groups ($\Delta T_{mean,water}$ using the first 2 FBGs and the others for $\Delta T_{mean,soil}$) is calculated and, then, the distances between the ΔT value of a given FBG and the two ΔT_{mean} values (thermal distances named TD_{water} and TD_{soil}) are computed:

$$TD_{water} = \left|\Delta T - \Delta T_{mean,water}\right|, \; TD_{soil} = \left|\Delta T - \Delta T_{mean,soil}\right| \quad (3)$$

As an example, FBG 1 has $\Delta T = 1.50$ °C and, thus, the distance between itself and $\Delta T_{mean,water}$ (equal to 1.45 °C) is $TD_{water} = 0.05$ °C, while the distance between itself and $\Delta T_{mean,soil}$ (equal to 5.27 °C) is $TD_{soil} = 3.77$ °C. This distance is a measure of similarity: the minimum of these values indicates the group in which the FBG must be placed. In this example, FBGs 3 and 4 need to change their group, from soil to water. At STEP 3, an iteration loop starts, in which STEP 2 is repeated until the new ΔT_{mean} values for both groups are the same as those at the previous step. At this point, the algorithm finds the final clusters and can provide an estimation of the riverbed level (STEP 4).

The next subsections treat at first a comparison between the results of the two proposed algorithms using the data collected in 2012 (Section 5.3) and, then, the comparison of the two methods with the results provided by the reference device, i.e., the echo sounder, employing the data collected in 2013 (Section 5.4). In the following, only the first nine sensors will be considered because the riverbed level never reaches the FBG 9. Nevertheless, the authors have verified that the number of sensors involved in the DC method does not influence the results if the first grouping (STEP 1) places in the water the first 2 sensors.

5.3. Results for 2012

The data collected in 2012 (267 datasets from September 4th to November 10th) are used here for checking whether the DC method (Section 5.2) provides results close to those given by the GK method (Section 5.1). Therefore, the focus here is not to understand whether the riverbed estimation is reasonable but on a crosscheck between the two proposed methods.

First of all, a ΔT threshold (ΔT_T) for method GK has to be found: referring to Fig. 8, the range of the grey area is approximately between 3.60 and 5.30 °C and, thus, the mean value, which is 4.45 °C, was selected as ΔT_T. FBGs with $\Delta T < \Delta T_T$ are considered in flowing water, otherwise they are considered as buried in the bed.

Considering the GK method, in 99.6% of the cases (266 cases out of 267) the procedure finds the riverbed level using the first check, i.e., comparing the results provided by ΔT and $\Delta\Delta T$. In 84% of these cases, $\Delta\tau$ provides the same result (even if it is not used; see Section 5.1). Only in one acquisition (September 30th at 8:56 AM, see also Fig. 11 discussed below), the three parameters are not in accordance one to each other and the riverbed level is evaluated with a worsened level of spatial accuracy. This case is showed in Fig. 11 because it is a significant example.

Looking at Fig. 11(a), it is easy to identify sensors in water (solid black curves) and buried in the bed (solid grey curves). Between them, there is the curve of FBG 4 (dashed red line). Its behavior needs an interpretation. A case like this was already discussed in the literature considering laboratory tests where an FBG was located close to the interface water-soil, regardless of its environment (either water or soil). If the FBG is in the water but close to the riverbed, the river velocity is close to zero in this area and, thus, the convection removes less heat because the dissipation is a function of the fluid velocity (see [39]). Therefore, the temperature increment is larger compared to the other sensors in water. Conversely, if the sensor is buried in the bed close to the interface, the heat exchange is mainly due to conduction, but with also a residual convection contribution which reduces the final ΔT. So far, the riverbed level was considered as a line that perfectly divides water and soil but, actually, the riverbed level is more like a layer with a thickness depending on the hydrodynamic condition of the river. In this layer, there are flowing water as well as solid transport so that the heat dissipation is a mix of convection and conduction processes hard to quantify. In this case, the ΔT analysis provides a riverbed level estimation between FBGs 4 and 5 while $\Delta\Delta T$ analysis indicates the riverbed level between FBGs 3 and 4. As discussed in section 5.1, being the result provided by $\Delta\tau$ different from those indicated by ΔT and $\Delta\Delta T$, the riverbed level is defined between sensors 3 and 5 (thus, with worsened spatial accuracy) which is the interval that includes the previous two. Hence, this case is something that can occur in practice because it is intrinsic in the BLESS working principle and in the physics of the natural system.

Considering the data of 2012, GK and DC methods always give results in accordance. In 266 cases out of 267, the same pair of consecutive FBGs define the riverbed level. In only a single case (see Fig. 11), the DC approach places the bed of the river between sensors 3 and 4, while the GK method places it between FBGs 3 and 5. However, also in this case, the results of the two methods are compatible. Fig. 12 shows the estimated riverbed level, together with the water level (measured by an ultrasonic radar) as a function of time. In this figure, the riverbed level is plotted as the mean value of the levels of the chosen adjacent FBGs. It is noticed that the date format in Fig. 12 has the day first and then the month (e.g., 5/9 is the 5th of September). The same applies for all the figures further in the manuscript.

Finally, the results of the two methods related to BLESS are compared to the reference transducer, i.e., the echo sounder, for the sake of completeness. Fig. 13 shows this comparison proving that the BLESS measurements are close to those of the echo sounder. In interpreting these results, one should also consider that the echo sounder measures over a given portion of river bed, while BLESS provides a punctual measurement. Furthermore, the two devices could measure in slightly different areas. Given these premises, the match between BLESS and

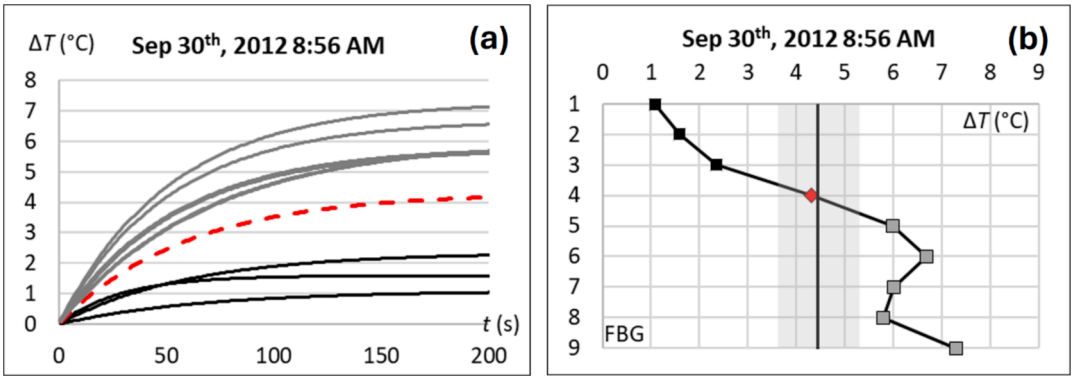

Fig. 11. Step response curves (a) and ΔT profile (b) of acquisition 103, September 30th 8:56 AM.

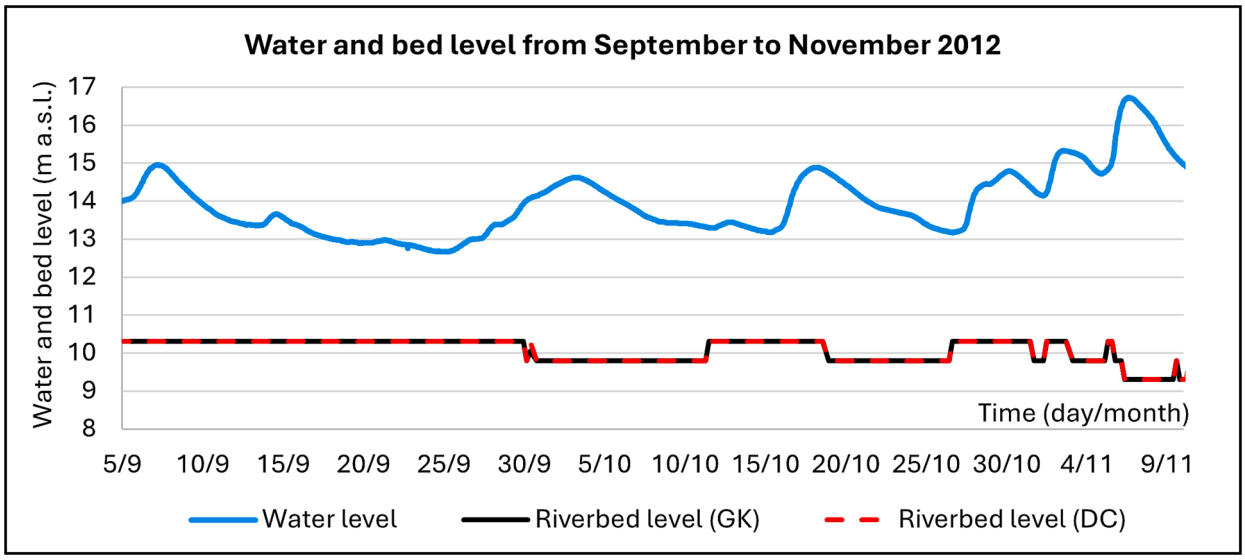

Fig. 12. Riverbed results and water level in 2012.

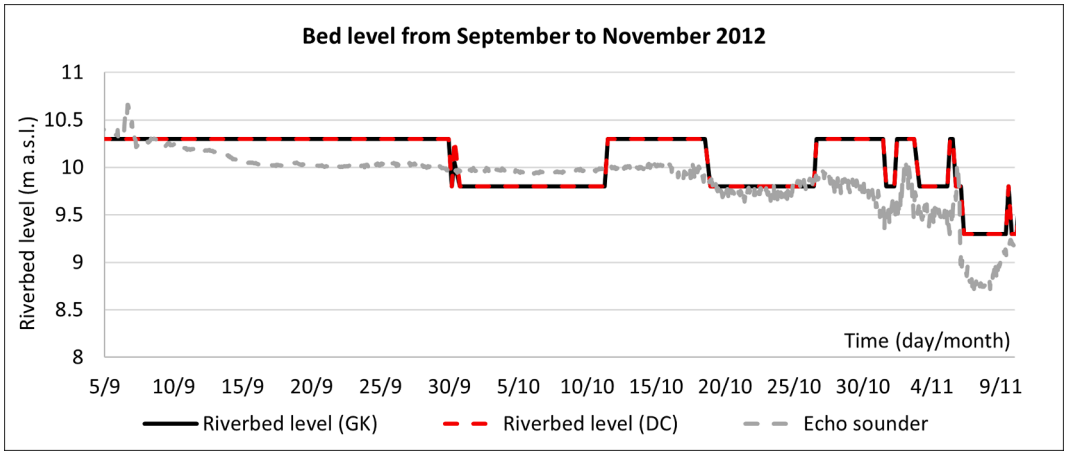

Fig. 13. Riverbed level estimates using either FBGs or echo sounder measurements during 2012.

echo sounder is satisfactory and similar trends are highlighted from all the curves in Fig. 13.

5.4. *Results for 2013*

Data collected in 2013 are now used to fully validate the methods developed for BLESS against the echo sounder results. The global results are shown in Fig. 14, where it comes out that DC method is always in good accordance with the echo sounder, while results of GK method are less in agreement with those of the other measurement methods and are characterized by a larger scatter. The whole datasets are divided into four periods, which are discussed in the next subsections, also providing an explanation for the differences shown by GK method compared to the other estimation approaches. Before proceeding, it is however worth

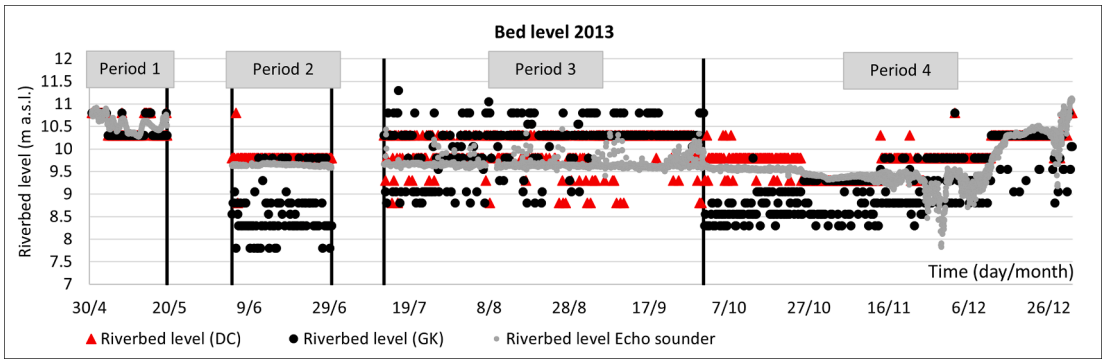

Fig. 14. Riverbed results in 2013 and identification of the four periods used for the analysis.

mentioning that the global bed level variations reckoned by the echo sounder, from about 11 m at the beginning of the acquisitions, down to nearly 9 m and up again to 11 m at the end of the measurement period, are similarly evidenced by BLESS employing the DC algorithm.

5.4.1. Period 1

In Period 1 (76 acquisitions), the echo sounder values are very close to those of the DC and GK algorithms. The largest differences between BLESS and echo sounder results are approximately equal to 50 cm. However, most of the times, this difference is much smaller, as evidenced in Fig. 15. In the 97% of the cases, GK method finds the riverbed level at the first evaluation stage (ΔT result equal to $\Delta\Delta T$ result), while $\Delta\tau$ gives results in accordance to those related to either ΔT or $\Delta\Delta T$ in the remaining 3% of the cases. The DC method agrees with the GK method in the 95% of the cases and, in the last 5%, the difference between the two methods is 50 cm.

Furthermore, Fig. 16 shows the ΔT values for the first nine FBGs, together with the ΔT threshold defined with the data collected in 2012 (see Section 5.3). All sensors, except FBG 3, have an almost constant value in time: FBGs 1 and 2 are in water and FBGs 4 to 9 are buried in the bed. FBG 3 is characterized by a continuous change of its ΔT because it is the only one that undergoes changes of the environment in which it is immerged, from soil to water and vice versa.

5.4.2. Periods 2 to 4

In periods 2 (100 acquisitions), 3 (318 acquisitions) and 4 (337 acquisitions), DC method is usually in good agreement with the echo sounder results, as show in Fig. 17.

Conversely, GK method often provides significantly different estimations of the bed level compared to the DC algorithm (see Fig. 18) in Periods 2 and 4, and thus also compared to the echo sounder. As an example, Fig. 18 shows that in Period 2 the GK method results are shifted downward compared to DC ones of approximately 1.5 m, also showing a larger result scatter.

The reason for this difference is related to the fact that during Period 2, one of the three electrical wires providing the thermal power failed, lowering the P value to about 1.0 W/FBG (loss of 33% of the total power). On the one hand, the DC method does not suffer of this problem, because of its automatic clustering capability. Conversely, GK method, based on the threshold value ΔT_T evaluated in 2012 with 1.5 W/FBG, obviously fails because of the mentioned change. This is also due to the physical base of the GK method.

The failure of the third electrical wire was proved by some electrical measurements carried out at the bridge (at the end of Period 2). Nevertheless, it can be deduced also analyzing, in Fig. 19, the trends of ΔT for the first nine FBGs. The ΔT values of the different FBGs are much closer each other compared to the case of Fig. 16, where all the three wires were properly working. Furthermore, the largest recorded ΔT values are smaller in Fig. 18 than in Fig. 16 (approximately 5.5 and 8 °C, respectively).

Two significant notes are worthy of attention. The first one is that in case the value of ΔT_T is lowered of 1/3 (thus, resulting equal to approximately 3.0 °C), the results of GK method improves and becomes comparable to those of the other two methods, as evidenced in Fig. 20. The second note is that the wrong results provided by the GK method in presence of a damage of BLESS does not imply that GK method is unreliable and only DC method must be used. Indeed, the comparison between DC and GK results allows achieving important pieces of information related to the health status of BLESS. When the two methods provide comparable results, BLESS works properly. Conversely, if the results diverge, it constitutes a warning about the possible presence of a damage/misfunctioning of BLESS. The nice property of DC method is that, as mentioned, it can properly estimate bed level even in case of damage due to absence of physical hypotheses for its functioning. Conversely, the working principle of GK method, based on physical assumptions, allows monitoring the health condition of BLESS.

During Period 3, the heating system was fully reactivated (see Fig. 18) but at the beginning of October 2013 (Period 4) one of three electrical cables of the power supply was lost permanently. This implies a good agreement of the results of the GK method with those of the other estimation approaches in Period 3 but not in Period 4. However, thanks to the comparison between DC and GK methods, the ΔT_T value could be modified, as done for Period 2, and GK results were realigned to DC results also in Period 4 (not plotted here for the sake of conciseness).

This analysis could be intended as suggesting that DC method is better than GK, so the latter can be considered irrelevant: nothing could be further from the truth. On the one hand, DC method is not based on physical assumptions so that it is always able to split sensors into two groups. On the other hand, the quality of the result of GK method is strictly correlated to the proper functioning of the heating system and this guarantees a physical interpretation of the results. These two methods acquire strength when they work together, as showed before.

Another important point is related to the echo sounder. In this paper its results are used as benchmark because (i) attention is focused on BLESS system and (ii) the echo sounder is a commercial device while BLESS is a prototype. Nevertheless, as mentioned in the introduction, also the echo sounder needs a data check and thus the comparison between BLESS and echo sounder is just to have an additional cross check to validate the DC and GK methods. Furthermore, the riverbed area targeted by the echo sounder is not in the same position of BLESS, so that slight differences are not only expected but also foreseen.

6. Conclusion

The paper has presented two different algorithms which can be fruitfully used for estimating river bed level at bridge piers when using BLESS system, which is a sedimeter based on Fiber Bragg Gratings heated by a properly designed electrical circuit through the Joule's

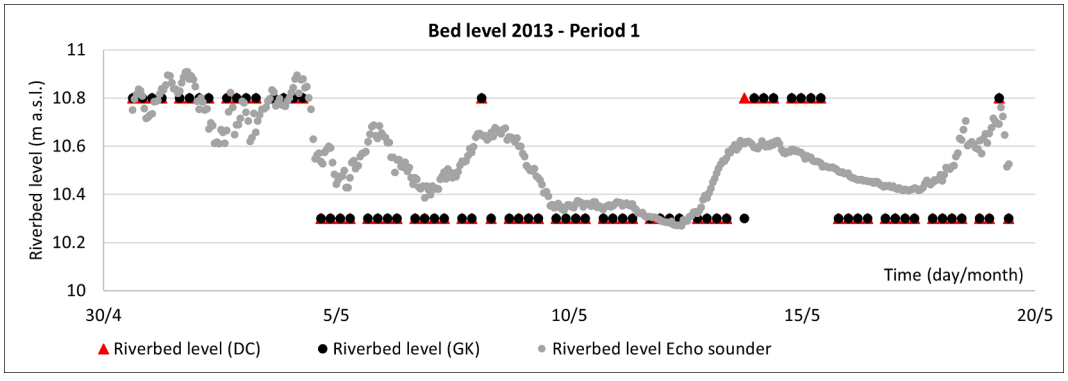

Fig. 15. Period 1 (see Fig. 14).

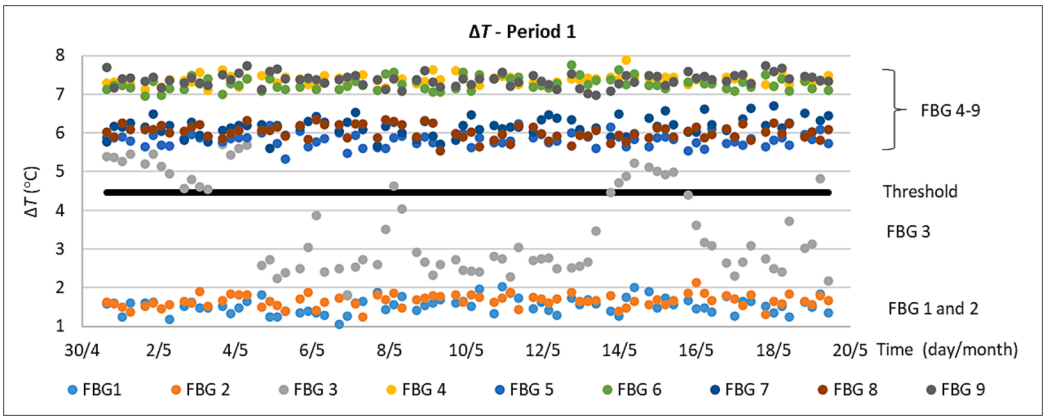

Fig. 16. ΔT values for the nine FBGs (Period 1).

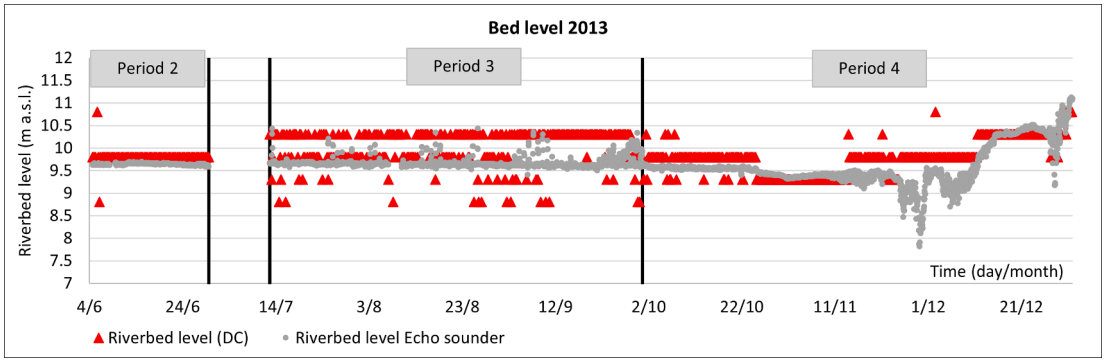

Fig. 17. Periods 2, 3 and 4 (only DC and echo sounder).

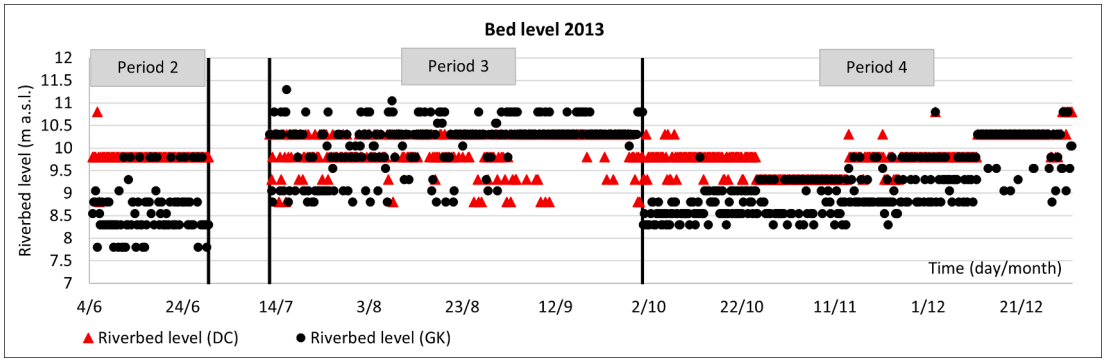

Fig. 18. Periods 2, 3 and 4 (only DC and GK methods).

effect.

The two methods, named GK and DC, are based on different approaches. The former is related to the estimation of three different parameters from the signals collected from the FBGs and is based on physical assumptions. The latter method relies on a data clustering approach and does not require any assumption about the system. This also implies that DC algorithm does not need to be trained, while GK method requires to use some data for training.

BLESS and a reference traditional device, i.e., an echo sounder, were compared at Borgoforte bridge on Po river. BLESS provided estimations of bed level characterized by a satisfactory agreement with echo sounder results, when DC algorithm is employed. GK method provides similar results when the operating conditions of BLESS are correct, while it shows significantly different results when a damage/misfunctioning occurs to BLESS. The use of the two estimation methods together, thus, allows obtaining important information about the correct functioning of BLESS, paving the way for new installations on real bridges.

It is also important to evidence that, at the moment, it is hard to obtain a fully detailed in-field comparison of a new river bed level measurement approach with a reference method. On the one hand, the measured quantity can be different between two different measurement approaches (as evidenced above for BLESS and the echo sounder) and, on the other hand, because no method can be currently considered as a reference.

CRediT authorship contribution statement

Gianluca Crotti: Writing – review & editing, Writing – original draft, Visualization, Validation, Software, Project administration, Methodology, Investigation, Formal analysis, Data curation, Conceptualization.

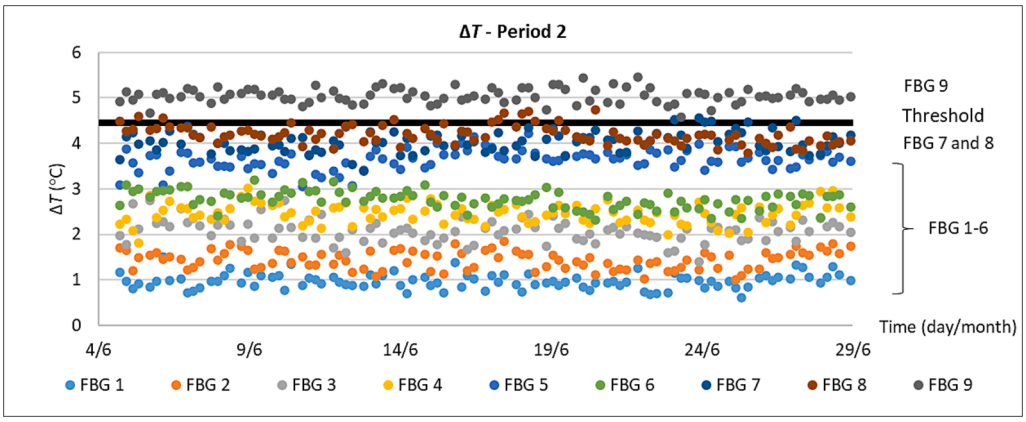

Fig. 19. ΔT values for the nine FBGs during Period 2. The black solid horizontal line represents the value of ΔT_T for P equal to 1.5 W/FBG.

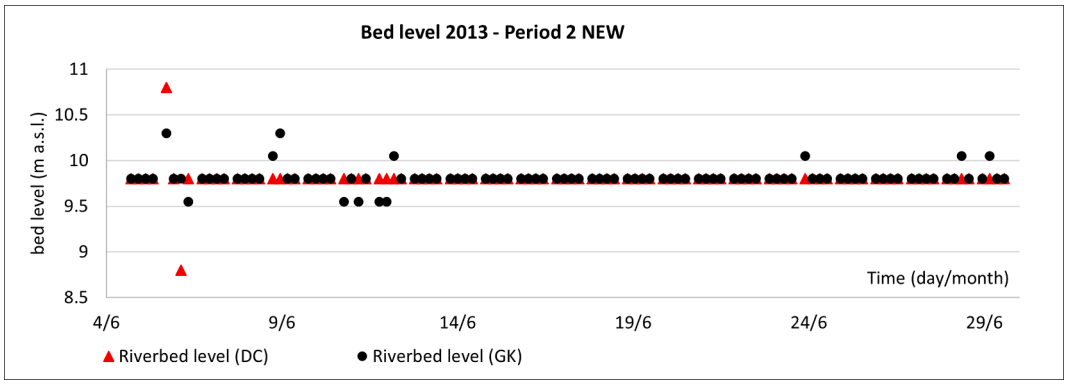

Fig. 20. DC and GK methods during Period 2 after updating the ΔT threshold due to the loss of one electrical cable.

Stefano Manzoni: Writing – review & editing, Writing – original draft, Validation, Methodology, Investigation, Formal analysis, Conceptualization.

Declaration of competing interest

The authors declare that they have no known competing financial interests or personal relationships that could have appeared to influence the work reported in this paper.

Acknowledgments

The authors would like to thank Daniele Cattani for his help in data analysis and development of DC algorithm. A special thank also to the Hydraulic laboratory "G. Fantoli" (Polytechnic of Milan). Furthermore, the authors would like to thank the Provincia di Mantova (Italy) for having partly funded this research project.

Data availability

The data that has been used is confidential.

References

[1] K. Wardhana, F.C. Hadipriono, Analysis of recent bridge failures in the United States, J. Perform. Constr. Facil 17 (3) (2003) 144–150, https://doi.org/10.1061/(asce)0887-3828(2003)17:3(144).
[2] J.L. Briaud, Scour depth at bridges: method including soil properties. I: maximum scour depth prediction, J. Geotech. Geoenviron. Eng. 141 (2) (2015) 1–13, https://doi.org/10.1061/(asce)gt.1943-5606.0001222.
[3] L.J. Prendergast, M.P. Limongelli, N. Ademovic, A. Anžlin, K. Gavin, M. Zanini, Structural health monitoring for performance assessment of bridges under flooding and seismic actions, Struct. Eng. Int. 28 (3) (2018) 296–307, https://doi.org/10.1080/10168664.2018.1472534.
[4] M. Pregnolato, P.J. Vardanega, M.P. Limongelli, P.F. Giordano, L.J. Prendergast, Risk-based bridge scour management: a survey. In: Bridge Maintenance, Safety, Management, Life-Cycle Sustainability and Innovations - Proceedings of the 10th International Conference on Bridge Maintenance, Safety and Management, IABMAS 2020 2021, pp. 693–701. https://doi.org/10.1201/9780429279119-91.
[5] A. Radice, O. Lauva, Live-bed pier scour in a covered flow, J. Hydraul. Eng. 143 (10) (2017) 1–8, https://doi.org/10.1061/(asce)hy.1943-7900.0001359.
[6] F. Ballio, A. Teruzzi, A. Radice, Constriction effects in clear-water scour at abutments, J. Hydraul. Eng. 135 (2) (2009) 140–145, https://doi.org/10.1061/(asce)0733-9429(2009)135:2(140).
[7] N. Yousefpour, S. Downie, S. Walker, N. Perkins, H. Dikanski, Machine learning solutions for bridge scour forecast based on monitoring data, Transp. Res. Rec. 2675 (10) (2021) 745–763, https://doi.org/10.1177/03611981211012693.
[8] J. Chambel, T. Fazeres-Ferradosa, F. Miranda, A.M. Bento, F. Taveira-Pinto, P. Lomonaco, A comprehensive review on scour and scour protections for complex bottom-fixed offshore and marine renewable energy foundations, Ocean Eng. 304 (April) (2024) 117829, https://doi.org/10.1016/j.oceaneng.2024.117829.
[9] K. Qu, D. Garcia Cava, S. Killbourn, A. Logan, Operational modal analysis for scour detection in mono-pile offshore wind turbines. In: P. Rizzo, A. Milazzo (Eds.) European Workshop on Structural Health Monitoring. EWSHM 2022. Lecture Notes in Civil Engineering, vol. 254, Springer, 2023. https://doi.org/10.1007/978-3-031-07258-1_67.
[10] Y. Liao, H. Wang, S. Hou, D. Feng, G. Wu, Identification of the scour depth of continuous girder bridges based on model updating and improved genetic algorithm, Adv. Struct. Eng. 25 (11) (2022) 2348–2363, https://doi.org/10.1177/13694332221095630.
[11] S. Tola, J. Tinoco, J.C. Matos, E. Obrien, Scour detection with monitoring methods and machine learning algorithms—A critical review, Appl. Sci. (Switzerland) 13 (3) (2023), https://doi.org/10.3390/app13031661.
[12] Y. He, J.P. Yang, Surrogate-assisted finite element model updating for detecting scour depths in a continuous bridge, J. Comput. Sci. 69 (February) (2023) 101996, https://doi.org/10.1016/j.jocs.2023.101996.
[13] NCHRP. Monitoring Scour Critical Bridges. Washington, DC: The National Academies Press, 2009. https://doi.org/10.17226/22979.
[14] P.A. Johnson, P.E. Clopper, L.W. Zevenbergen, P.F. Lagasse, Quantifying uncertainty and reliability in bridge scour estimations, J. Hydraul. Eng. 141 (7) (2015) 1–9, https://doi.org/10.1061/(asce)hy.1943-7900.0001017.

[15] R. Lamb, W. Aspinall, H. Odbert, T. Wagener, Vulnerability of bridges to scour: insights from an international expert elicitation workshop, Nat. Hazards Earth Syst. Sci. 17 (8) (2017) 1393–1409, https://doi.org/10.5194/nhess-17-1393-2017.
[16] M. Farooq, N. Banthia, F. Azhari, Bridge scour monitoring: challenges and opportunities. In: IABSE Conference, Vancouver 2017: Engineering the Future - Report, 2017.
[17] S. Laflamme, Perspective on structural health monitoring of bridge scour, Meas. Sci. Technol. 35 (5) (2024), https://doi.org/10.1088/1361-6501/ad23be.
[18] M. Farooq, F. Azhari, N. Banthia, Photoelectric sensors for wireless monitoring of bridge scour–laboratory investigation and field validation, Struct. Infrastruct. Eng. (2023) 1–12, https://doi.org/10.1080/15732479.2023.2261434.
[19] M. Amirmojahedi, S. Akib, H. Basser, C.R. Ooi, Methods for monitoring scour from large-diameter heat probe tests, Struct. Health Monit. 15 (1) (2016) 38–49, https://doi.org/10.1177/1475921715620004.
[20] M. Farooq, F. Azhari, N. Banthia, A state-of-the-art review of active-thermometry techniques for bridge and pipeline scour monitoring, and exploratory passive thermometry studies, J. Struct. Integrity Maint. 8 (2) (2023) 67–78, https://doi.org/10.1080/24705314.2023.2165471.
[21] K. Wang, C.P. Lin, C.C. Chung, A bundled time domain reflectometry-based sensing cable for monitoring of bridge scour, Struct. Control Health Monit. 26 (5) (2019) 1–14, https://doi.org/10.1002/stc.2345.
[22] M.L. Funderburk, J. Tran, M.D. Todd, A. Netchaev, K.J. Loh, Active scour monitoring using ultrasonic time domain reflectometry of buried slender sensors, Smart Mater. Struct. 31 (1) (2022), https://doi.org/10.1088/1361-665X/ac3da0.
[23] Y. Chen, F. Tang, Z. Li, G. Chen, Y. Tang, Bridge scour monitoring using smart rocks based on magnetic field interference, Smart Mater. Struct. 27 (8) (2018) 85012, https://doi.org/10.1088/1361-665X/aacbf9.
[24] S. Jiang, Q. Wang, W. Sun, Y. Tan, Bridge scour monitoring using smart magnetic rock, Measurement 205 (2) (2022) 112175, https://doi.org/10.1016/j.measurement.2022.112175.
[25] A. Malekjafarian, C.W. Kim, E.J. OBrien, L.J. Prendergast, P.C. Fitzgerald, S. Nakajima, Experimental demonstration of a mode shape-based scour-monitoring method for multispan bridges with shallow foundations, J. Bridg. Eng. 25 (8) (2020) 1–13, https://doi.org/10.1061/(asce)be.1943-5592.0001586.
[26] J. Zhan, Y. Wang, F. Zhang, Y. An, K. Liu, Scour depth evaluation of highway bridge piers using vibration measurements and finite element model updating, Eng. Struct. 2022 (253) (2021) 113815, https://doi.org/10.1016/j.engstruct.2021.113815.
[27] M.L. Funderburk, S.K. Huang, C.H. Loh, K.J. Loh, Densely distributed and real-time scour hole monitoring using piezoelectric rod sensors, Adv. Struct. Eng. 22 (16) (2019) 3395–3411, https://doi.org/10.1177/1369433219831124.
[28] A.M. Bento, L. Couto, T. Viseu, J.P. Pêgo, Image-based techniques for the advanced characterization of scour around bridge piers in laboratory, J. Hydraul. Eng. 148 (6) (2022) 1–8, https://doi.org/10.1061/(asce)hy.1943-7900.0001981.
[29] C. Wang, X. Yu, F. Liang, A review of bridge scour: mechanism, estimation, monitoring and countermeasures, Nat. Hazards 87 (3) (2017) 1881–1906, https://doi.org/10.1007/s11069-017-2842-2.
[30] F. De Falco, R. Mele, The monitoring of bridges for scour by sonar and sedimetri, NDT and E Int. 35 (2) (2002) 117–123, https://doi.org/10.1016/S0963-8695(01)00031-7.
[31] G. Crotti, Decision Support System for hydraulic risk management of a river bridge - PhD thesis. Politecnico di Milano, 2020.
[32] Y.B. Lin, J.C. Chen, K.C. Chang, J.C. Chern, J.S. Lai, Real-time monitoring of local scour by using fiber Bragg grating sensors, Smart Mater. Struct. 14 (4) (2005) 664, https://doi.org/10.1088/0964-1726/14/4/025.
[33] R. Hatley, M. Shehata, C. Sayde, C. Castro-Bolinaga, High-resolution monitoring of scour using a novel fiber-optic distributed temperature sensing device: a proof-of-concept laboratory study, Sensors (Basel, Switzerland) 23 (2023), https://doi.org/10.3390/s23073758.
[34] X. Zhang, X. Zhao, Research on subsea pipeline scour monitoring using distributed Raman optical sensing technique, Proc. SPIE-Int. Soc. Opt. Eng. 10598 (2018), https://doi.org/10.1117/12.2296557.
[35] X. Kong, S.C.M. Ho, G. Song, C.S. Cai, Scour monitoring system using fiber Bragg grating sensors and water-swellable polymers, J. Bridg. Eng. 22 (7) (2017) 1–11, https://doi.org/10.1061/(asce)be.1943-5592.0001062.
[36] W. Liu, W. Zhou, H. Li, Bridge scour estimation using unconstrained distributed fiber optic sensors, J. Civ. Struct. Heal. Monit. 12 (4) (2022) 775–784, https://doi.org/10.1007/s13349-021-00510-y.
[37] D. Ba, B. Wang, D. Zhou, M. Yin, Y. Dong, H. Li, et al., Distributed measurement of dynamic strain based on multi-slope assisted fast BOTDA, Opt. Express 24 (9) (2016) 9781, https://doi.org/10.1364/oe.24.009781.
[38] A. Zarafshan, A. Iranmanesh, F. Ansari, Vibration-based method and sensor for monitoring of bridge scour, J. Bridg. Eng. 17 (6) (2012) 829–838, https://doi.org/10.1061/(asce)be.1943-5592.0000362.
[39] S. Manzoni, G. Crotti, F. Ballio, A. Cigada, F. Inzoli, E. Colombo, Bless: a fiber optic sedimeter, Flow Meas. Instrum. 22 (5) (2011) 447–455, https://doi.org/10.1016/j.flowmeasinst.2011.06.010.
[40] B.M. Basma, D. Piétroy, M.I. Boukhari, Z. Chahbi, T. Blanchet, J.P. Chatelon, et al., On thermal characterization method of integrated magnetic components, Sci. Rep. 14 (1) (2024) 1–12, https://doi.org/10.1038/s41598-024-54588-7.
[41] M. Ahmed, Y. Matsumoto, R. Yoon, S. Takahashi, Y. Sanada, Accurate measurement of the bond stress between rebar and concrete in reinforced concrete using FBG sensing technology, Sci. Rep. 14 (1) (2024) 1–11, https://doi.org/10.1038/s41598-024-52555-w.
[42] X. Han, H. Zhong, K. Li, X. Xue, W. Wu, N. Hu, et al., Operando monitoring of dendrite formation in lithium metal batteries via ultrasensitive tilted fiber Bragg grating sensors, Light Sci. Appl. 13 (1) (2024), https://doi.org/10.1038/s41377-023-01346-5.
[43] C. Xu, L. Li, R. Hu, H. Wu, L. Kong, N. Zhong, et al., In situ detection of spatial distribution information of temperature-pH-strain of sandstone cultural relics, Npj Mater. Degrad. 8 (1) (2024) 1–11, https://doi.org/10.1038/s41529-024-00438-w.
[44] Y. Ma, P. Chen, C. Yang, Z. Cheng, L. Xiao, Development and experimental validation of an FBG-based substructure cross-sectional load measurement approach for a semi-submersible floating wind turbine, Eng. Struct. 2024 (303) (2023) 117527, https://doi.org/10.1016/j.engstruct.2024.117527.
[45] M. Sypabekova, A. Amantayeva, A. Gonzalez-Vila, M. Shaimerdenova, C. Caucheteur, D. Tosi, Spectral characteristics and interrogation of a fiber-optic ball resonator biosensor modulated by a tilted fiber Bragg grating, Opt. Fiber Technol. 79 (March) (2023) 103354, https://doi.org/10.1016/j.yofte.2023.103354.
[46] F. Ballio, G. Ballio, S. Franzetti, G. Crotti, G. Solari, Actions monitoring as an alternative to structural rehabilitation: case study of a river bridge, Struct. Control Health Monit. 25 (11) (2018) 1–22, https://doi.org/10.1002/stc.2250.
[47] G. Crotti, A. Cigada, Scour at river bridge piers: real-time vulnerability assessment through the continuous monitoring of a bridge over the river Po, Italy, J. Civ. Struct. Heal. Monit. 9 (4) (2019) 513–528, https://doi.org/10.1007/s13349-019-00348-5.
[48] A. Cigada, F. Ballio, Inzoli F. Hydraulic monitoring unit. WO2009013151A1, 2009.
[49] E. Doebelin, Measurement Systems: Application and Design, McGraw-Hill, New York, 2003.
[50] S. James, L. Dockney, R. Tatam, Simultaneous independent temperature and strain measurement using in-fibre Bragg grating sensors, Electron. Lett 32 (12) (1996) 1133–1134, https://doi.org/10.1049/el:19960732.
[51] J. MacQueen, Some methods for classification and analysis of multivariate observations. In: Proceedings of the 5th Berkeley Symposium on Mathematical Statistics and Probability, vol. 1, University of California Press, Berkeley (USA), 1967. https://doi.org/10.1007/s11665-016-2173-6.